Pairings and Polarities of the 14 Strands in Sickle Cell Hemoglobin Fibers

David W. Rodgers, Richard H. Crepeau, Stuart J. Edelstein

Proceedings of the National Academy of Sciences of the United States of America, Volume 84, Issue 17 (Sep. 1, 1987), 6157-6161.

Stable URL:
http://links.jstor.org/sici?sici=0027-8424%2819870901%2984%3A17%3C6157%3APAPOT1%3E2.0.CO%3B2

Proc. Natl. Acad. Sci. USA
Vol. 84, pp. 6157–6161, September 1987
Biophysics

Pairings and polarities of the 14 strands in sickle cell hemoglobin fibers

(hemoglobin S fibers/electron microscopy/image reconstruction)

DAVID W. RODGERS*, RICHARD H. CREPEAU†, AND STUART J. EDELSTEIN‡

Section of Biochemistry, Molecular and Cell Biology, Wing Hall, Cornell University, Ithaca, NY 14853

Communicated by Leon A. Heppel, May 4, 1987

ABSTRACT **Sickle cell anemia results from the formation of hemoglobin S fibers in erythrocytes, and a greater understanding of the structure of these fibers should provide insights into the basis of the disease and aid in the development of effective antisickling agents. Improved reconstructions from electron micrographs of negatively stained single hemoglobin S fibers or embedded fiber bundles reveal that the 14 strands of the fiber are organized into pairs. The strands in each of the seven pairs are half-staggered, and from longitudinal views the polarity of each pair can be determined. The positions of the pairs and their polarities (three in one orientation; four in the opposite orientation) suggest a close relationship with the crystals of deoxyhemoglobin S composed of antiparallel pairs of half-staggered strands.**

The dramatic transformation of erythrocytes caused by the sickle mutation of hemoglobin is due to the association of the hemoglobin S (HbS) molecules into long fibers that align to distort the cell shape. Understanding the self-association of HbS molecules has been the goal of extensive research activity, with studies of the fiber structure by electron microscopy (1) and crystallographic investigations of HbS (2) both providing considerable information. The fiber structure is a complex helical assembly of 14 strands of HbS molecules with a core of 4 strands surrounded by 10 outer strands in a roughly hexagonal packing. The crystals of HbS appear to be related to the fibers, since the valine-β6 residue and other residues implicated in intermolecular contacts of the fibers lie at contacts in the crystals (see refs. 3 and 4). However, the exact relationship between the strands of the fibers and those present in the crystals has remained elusive. Defining this relationship would permit the detailed structural information available for the crystal to be applied to analysis of the complex molecular interactions in the fiber.

A study of rare incomplete fibers has demonstrated that the absence of strands occurs in pairs (5), implying the existence of tightly associated double strands. The strands of each pair are staggered by half of a molecular diameter with respect to each other, and hence are possibly related to half-staggered strands also present in the crystal. In the absence of direct information on pairing and strand-pair polarity in the reconstructed images, however, it has not been possible to relate the crystal and fiber structures definitively. A tentative model was proposed that includes the introduction of the transformations necessary to convert linear to helical strands (4). While this model clarified certain aspects of the problem, particularly the role of α-chain mutations that influence fiber formation, additional information on strand pairing and polarity was needed. Such information would serve also to resolve questions raised by other laboratories concerning the possibility of 16-strand structures (6) or a 14-strand structure with other pairing arrangements (7). Improved images of negatively stained fibers and the development of new computational approaches involving fiber straightening and cross-correlation algorithms (8) have now made it possible to clarify the remaining issues of the fiber structure. We present here reconstructions that demonstrate directly both the pairings of the strands and the polarity of each pair.

Fiber Preparation and Image Analysis

The fibers used in these studies were assembled from purified HbS and prepared for electron microscopy by either of two methods. The first preparation technique involved negatively staining fibers on carbon-coated grids as described (5). Individual fibers adhered to the carbon and were allowed to dry after excess stain had been removed. In addition to this adhesion method, a more elaborate embedding and thin-sectioning procedure was developed to insure stabilization of the fiber structure during preparation. This embedding method has proven particularly successful when applied to bundles of HbS fibers produced by stirring concentrated solutions during polymerization (9). Cross-linking and stabilization of the fiber bundles was achieved by infiltration with a glutaraldehyde/tannic acid mixture (10, 11) and subsequent exposure to osmium tetroxide in solution. Thus stabilized, the specimens were dehydrated and embedded in an epoxy-type resin. Thin sections were cut through randomly oriented bundles, stained (negatively), and screened in the electron microscope to locate areas that contained only a single layer of fibers. Examples of electron micrographs obtained from HbS fibers prepared by the two methods are presented in Fig. 1*a*. Both samples exhibit the characteristic alternating wide and narrow regions that result from viewing the elliptical fiber cross section as it rotates along the helix. The complex architecture of these polymers is indicated by the considerable internal detail visible in the fiber images.

The adhesion method of preparation described above was successfully used in early studies to determine some aspects of the fiber structure; however, image analysis was limited to short regions of the available fiber length by curvature and variations in the helical pitch. We have utilized fiber straightening and cross-correlation techniques to overcome these limitations, allowing areas that repeat along the length of a fiber to be averaged. This averaging procedure substantially improves the quality of images available for three-dimensional reconstruction.

The publication costs of this article were defrayed in part by page charge payment. This article must therefore be hereby marked "*advertisement*" in accordance with 18 U.S.C. §1734 solely to indicate this fact.

Abbreviation: HbS, hemoglobin S.

*Present address: Department of Biochemistry and Molecular Biology, Harvard University, Cambridge, MA 02138.
†Present address: Department of Chemistry, Cornell University, Ithaca, NY 14853.
‡To whom reprint requests should be addressed at the present address: Department of Biochemistry, University of Geneva, Sciences II, CH-1211 Geneva 4, Switzerland.

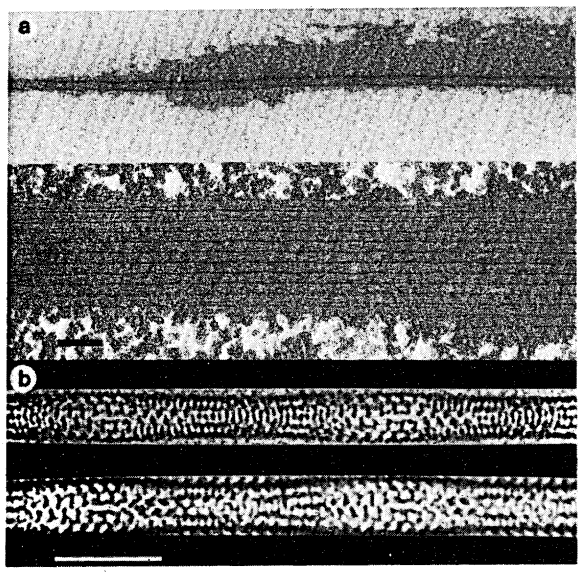

FIG. 1. Micrographs and image analysis of HbS fibers. (*a*) Micrographs of negatively stained HbS fibers prepared for electron microscopy by an adhesion method or embedding. HbS was purified by the method of Huisman and Dozy (12) (with minor modifications) and polymerized at pH 7.1 by warming to room temperature after deoxygenation under nitrogen. (*a Upper*) Fiber prepared by negative staining with 2% phosphotungstate and allowed to adhere to carbon-coated grids as excess stain was removed (5). (*a Lower*) Image of a thin section through a bundle containing many aligned fibers that was produced by stirring a solution of HbS during polymerization (9). A sample of bundles was fixed in 2.5% glutaraldehyde/4% tannic acid for ≈12 hr, washed, and then exposed to 1% osmium tetroxide for 1 hr. The bundles were then dehydrated with ethanol, embedded in Spurr resin, and thin-sectioned for viewing in the electron microscope. (Bar, 1000 Å.) (*b*) Fiber images produced by averaging views that repeat along the length of the fibers. A cross-correlation technique (8) was used to locate the repeating areas on fibers that had been computationally straightened by using the algorithm described in the text. (*b Upper*) Image from a single negatively stained fiber. (*b Lower*) An average image of three fibers from the thin section of a fiber bundle. Computed Fourier transforms of these images have significant reflections extending to about 25-Å resolution. The average image from the fiber prepared by the adhesion method is narrower than the embedded fiber average image and has a shorter helical repeat distance. Repeat lengths are known to vary for adhesion-prepared fibers (1, 5, 8), and both the adhesion and embedding methods used in these studies produced fibers with repeat distances that were within the previously observed range. The widths of the fibers were consistent with earlier measurements from adhesion-prepared fibers and with measured center-to-center spacings of fibers in cross sections of embedded bundles (11, 13). The edges of adjacent fibers in the bundle are visible at the top and bottom of the lower image. (Bar, 500 Å.)

The straightening algorithm first generates a smooth curve through the center of the original fiber using points chosen interactively. Then for each point (X,Y) of the straightened image, the distance X along the curve and the distance Y perpendicular to the curve define the equivalent point in the curved image. This method assumes that the fiber curvature is continuous, with no sharp breaks.

Once the fiber images had been straightened, a cross-correlation technique (8) was used to locate repeating areas along the helix. The equivalent areas could then be averaged, increasing the signal-to-noise ratio of the data. Use of cross-correlation permitted compensation for shifts in the positions of these areas due to slight variations in the helical repeat. Differences between equivalent areas that resulted from the pitch variations were negligible if sufficiently small regions (approximately one-third of a fiber repeat) were chosen for correlation. A full repeat of the fiber was then reconstructed by appending several of these smaller averages. Images produced in this manner from HbS fibers prepared by adhesion or embedding are presented in Fig. 1*b*. Agreement between the adhesion-prepared and the embedded fibers is apparent, and these averages demonstrate a dramatic increase in detail over both the original images and those obtained in a previous study by Fourier filtering single-fiber repeats (1). As a result, reconstructions based on the improved images have provided new information about the interactions and directionality of the 14 strands present in the HbS fibers.

Strand Number and Pairings

The HbS fiber can be described by a stack of identical, 64-Å-thick disks, with each successive disk rotated by about 7° with respect to its predecessor. At least 20 independent views of this repeating unit are present in the full helical rotation of ≈3000 Å. From these independent views, the three-dimensional structure of the fiber unit repeat was reconstructed by using the real-space EFIRT algorithm of Crowther and Klug (14). By untwisting and projecting this reconstruction onto a plane perpendicular to the helix axis, an average cross section or end-on view of the fiber was calculated. Cross-sectional projections obtained from the average images of fibers prepared by adhesion or embedding are presented in Fig. 2*a*. The 14-strand nature of the HbS fibers is evident in both cases, confirming the reconstructions produced from single helical repeats in earlier studies (1, 5). Determination of a 14-strand structure for the embedded preparations is particularly significant, since structural rearrangement of the internal fibers in a stabilized and cross-linked bundle is less likely than with single fibers prepared by the adhesion method.

In addition to confirming the 14-strand structure, the end-on views obtained from average images provide the first

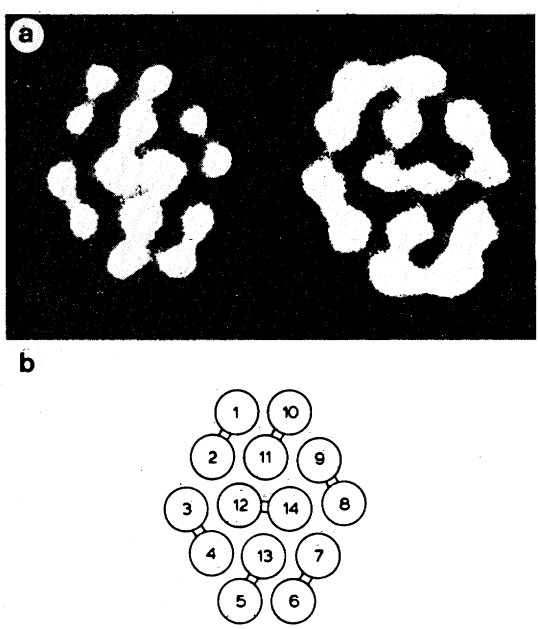

FIG. 2. Organization of the strands in the HbS fibers. (*a*) End-on views calculated from correlated images of fibers prepared by the adhesion method (*Left*) or embedding (*Right*). The 64-Å repeating unit of the helix was reconstructed as a number of two-dimensional slices perpendicular to the fiber axis by using the EFIRT algorithm of Crowther and Klug (14). To produce these average cross sections, the slices making up the unit repeat were corrected for rotation due to the helical twist, averaged, and viewed down the fiber axis. (*b*) Proposed pairing of strands based on a previous analysis of incomplete fibers (5).

direct evidence for the pairing of strands in the fiber. Particularly in the embedded fibers, each strand is now seen to be joined to an adjacent strand by a bridge of protein density, which indicates a close, stain-excluding interaction. This association into pairs is reflected in the relative strand positions in the cross section. The average center-to-center distance between strands joined by bridging densities is 16% less than the average distance between all neighboring strands. Based on this proximity of molecular centers and the presence of stain excluding contacts, strands can be assigned to the pairs 1–2, 3–4, 5–13, 6–7, 8–9, 10–11, and 12–14. Analysis of incomplete fibers has led to the proposal of exactly this pairing scheme in an earlier study (Fig. 2*b*) (5).

Relation to Crystal Pairs and Polarity

The presence of paired strands in both the fibers and crystals (2) of HbS suggests a possible relationship between the two structures. If these pairs are equivalent, then a detailed model of the fiber could be constructed from the high-resolution information available for the crystal. Their similarity is supported by a strong resemblance between the bilobed pairs seen in the embedded fiber cross section (Fig. 2*a*) and the end-on views of paired strands reported for negatively stained HbS crystals (15). The improved reconstructions from average images now allow more extensive comparisons to be made between the crystal and fiber pairs.

The strands within each crystal pair are shifted with respect to each other by half a molecular diameter along the pair axis. Therefore, the extent to which the fiber pairs are also half-staggered is an important measure of similarity. By tracing strands in the reconstructions along their helical path, the relative stagger within each pair of the fiber may be determined. These spacings are presented in Table 1 as distances along the helical axis of each pair. When the spacings along the pair axes are compared to the value of 31.7 Å for the average stagger of pairs in the crystal (2), the agreement is excellent.

The similarity of crystal and fiber pairs can be evaluated in greater detail by examining each from a direction perpendicular to both the strands of the pair and the line connecting their centers. This view of a crystal pair and a representation of the projected electron density, which has an appearance similar to the pairs in negatively stained crystals viewed from this perspective (15), are diagrammed in Fig. 3*a*. To obtain the corresponding view of the fiber pairs, each double strand was isolated from the three-dimensional reconstruction, corrected for the helical path, and projected to a plane through the center of the strands and parallel to their axes. Examples of these projections, obtained from an adhesion-prepared fiber, are presented in Fig. 3*b*. When these views, or those from embedded fibers, are compared to the projected crystal electron density, their overall similarity is striking, and a number of common features can be identified. Stain

Table 1. Stagger between paired strands in the fiber

Pair	Stagger, Å	Pair	Stagger, Å
1–2	32.7	5–13	31.2
3–4	31.5	10–11	32.7
6–7	33.0	12–14	31.5
8–9	31.6		

The differences in molecular center positions along the fiber for the two strands in each pair are reported as their separation along the helical axis of the pair. These spacings are an average of the values from 14 embedded and adhesion-prepared specimens and may be compared to the 31.7-Å average stagger of paired strands in the crystal (2). (The crystal strands are not precisely half-staggered, giving rise to two axial spacing values for the pairs. Since this small deviation from the half-staggered position cannot be detected in the fiber data, an average of the two values from the crystal is used for comparison.)

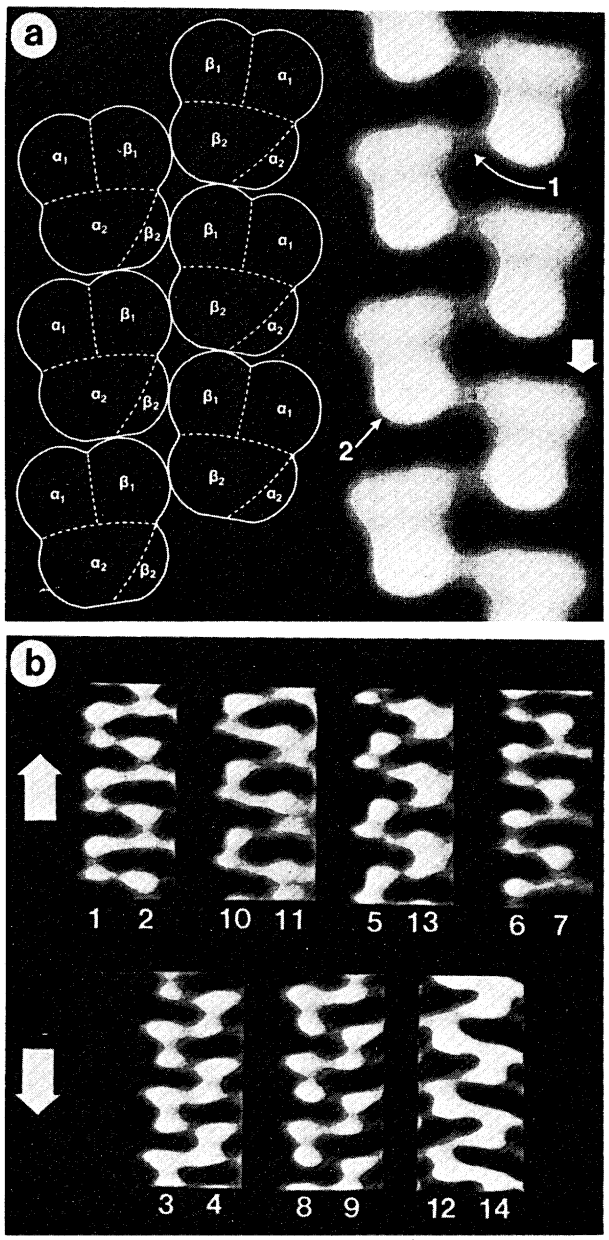

FIG. 3. Side view of the paired strands. (*a*) Diagram of a crystal pair viewed down the *c* axis (*Left*) and a representation of the projected electron density (*Right*), which closely resembles negatively stained crystal pairs (15). Even at low resolution, distinctive features of the double strands are present in this view. The strong cross-bridges connecting opposing strands are seen, as indicated for a pair of molecules by arrow 1. Also, the tilt of the HbS molecules with respect to the strand axis is visible. As a result of the superposition of the α_2 and β_2 subunits in this view, one half of each molecule appears as a stronger, more compact density. The position of this strong density is indicated by arrow 2 for one HbS tetramer. The asymmetric projection and the tilt of the molecules result in an overall polarity for the pairs. For reference, the crystal pair shown here will be considered to point toward the bottom of the page (see the arrow beside the projected density representation on the right). (*b*) Seven paired strands from a reconstruction of an adhesion-prepared HbS fiber. The pairs have been isolated and corrected for helical twist to allow comparison with crystal pairs. Numbers below each pair identify the strand according to the convention shown in Fig. 2*b*. Arrows indicate the polarity of the pairs in each row as defined in *a*.

penetration is generally sufficient to permit the interface between the α_1–β_1 and the α_2–β_2 dimers in the HbS molecules to be discerned, and, in many cases, the strong density projection corresponding to the superposition of the α_2 and β_2 subunits is visible. These features are consistent with the structure of the crystal pairs. The tilt of the tetramers with respect to the strand axes seen in the crystal is also reproduced clearly in the fiber reconstructions. Thus, the HbS molecules in the strands of untwisted fiber pairs appear to have the same orientation as in the crystal strands. In addition, the bridging densities that result from the contacts between strands are identical to those in the crystal projections. Therefore, the pairs in the fiber are indistinguishable from crystal pairs at the resolution of the reconstructions.

As mentioned above, the long axis of each HbS molecule in the crystal is slightly canted with respect to the strand axis. This tilt, together with the asymmetry of the projected molecular protein density, gives the double strands a marked polarity when viewed along the crystal *c* axis (see Fig. 3*a*). The presence of these features in the improved reconstructions has permitted an important aspect of the fiber structure, the directionality of the pairs, to be addressed. The pairs in a total of 14 embedded or adhesion-prepared fibers were examined. The most useful measure of polarity was the angular orientation of the HbS molecules. Presence of a strong density resulting from the superimposed α_2 and β_2 subunits often supported the assignment of directionality but was a less consistent feature of the reconstructions. On the basis of these criteria, three pairs (3–4, 8–9, and 12–14) were found to possess a common polarity, while the remaining four pairs (1–2, 6–7, 5–13, and 10–11) had the opposite orientation. The polarities of a small number of pairs could not be judged unambiguously; however, when an orientation could be determined, it always agreed with these assignments. The pairs in Fig. 3*b* illustrate the determination of polarity. As indicated by the arrows, the four pairs in the top row have all been assigned a polarity opposite to that of the model pair shown in Fig. 3*a*, and the three pairs on the bottom are oriented in the same direction as the model. If the strands are traced in the direction of the arrows, HbS molecules tilt toward the center of the pair, and overlapping α_2 and β_2 subunits are located in the distal half of each tetramer.

Information on polarity, as well as strand pairing, is summarized in Fig. 4*a*. This diagram models the fiber cross section as it would appear if viewed from the bottom of the correlated image in Fig. 4*b*, with pairs appearing as bilobed outlines and polarity indicated by the presence or absence of hatching. In this view, the absolute direction of the hatched pairs, as defined by the arrows in Fig. 3, is into the page. Some of the features of this cross section can be readily interpreted in certain regions of the correlated image. At the position labeled A in the average image, the fiber presents a narrow aspect with four longitudinal striations as a prominent feature. This view corresponds to a projection of the cross section in the direction indicated by the arrow marked A. The axial striations can be seen to arise from the superposition of four lines of strands: 1–2–3, 10–11–12–4, 9–14–13–5, and 8–7–6. Four striations running parallel to the fiber also appear at the point labeled B. Again, the image results from the overlap of strands, but in this case, when the fiber is viewed in the direction of arrow B. Although both this area and the region marked A show four parallel striations, close inspection reveals differences in their appearance. Many of these differences can be directly attributed to the association of strands into pairs, which moves their centers off a strictly hexagonal lattice in the cross section. For example, pairing causes the center-to-center distances between strand 9 and the 10–11 pair and between strand 4 and the 5–13 pair to be relatively large when viewed in the direction of the arrow A. The corresponding view in the B direction is dominated by the closely spaced strands in the 1–2 and 6–7 pairs. These differences in strand separation result in the two center striations in region A being more widely separated than those in region B.

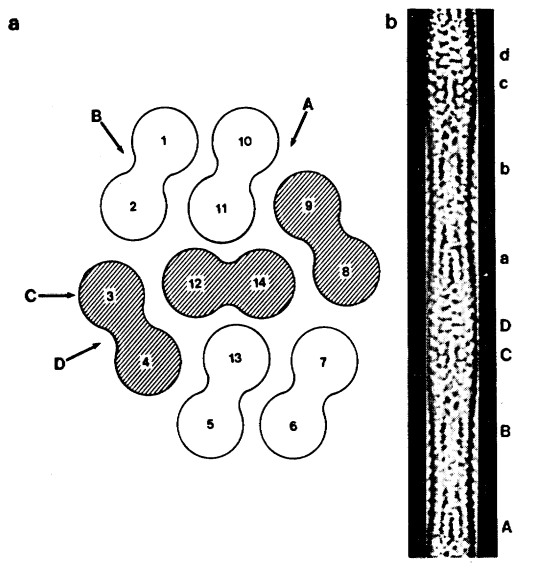

FIG. 4. Relationship of the fiber image to strand pairing and polarity. (*a*) Model of the fiber cross section based on reconstructions from average images. Paired strands are shown as bilobed densities, and the direction of each pair is indicated by the presence or absence of hatching. Arrows A–D denote directions of view that can be interpreted easily in images of the fiber as described in the text. (*b*) Correlation-averaged image of a HbS fiber. Areas A–D correspond to projections of the fiber along the directions indicated by the arrows in *a*. Areas corresponding to views along the directions opposite to the arrows are denoted a–d.

The effects of double-strand polarity are also easily related to features present in some portions of the image. In the region labeled C, the superposition of strands in the C direction gives the appearance of five axial striations. The predominant contribution to the two strands on each side comes from, in one case, the 1–2 and 10–11 pairs, and in the other, the 5–13 and 6–7 pairs. Since the two pairs of each set have the same polarity and axial position, their orientation is directly visible in the image. By tracing the image in Fig. 4*b* from top to bottom, the projected densities of the HbS molecules can be observed to tilt toward the center of each set of two outer strands, indicating that the four pairs run in this direction. Tilting of protein densities also occurs near the center of the fiber at position D, but with an opposite orientation. Here it reflects the polarities of the remaining three pairs when viewed along arrow D. Thus, the polarities as well as the pairings deduced for the 14 strands are consistent with the features of the fiber images.

Discussion

The data presented here confirm the 14-strand structure of the HbS fibers derived in an earlier study (1) and provide the first direct structural evidence for the arrangement of strands into seven tightly associated pairs. Sufficient detail is present in the three-dimensional reconstructions to allow each pair of the fiber to be assigned a polarity, with four pairs of like orientation and three pairs of opposite polarity. The pairs of strands are shown to have many features in common with those found in crystals of HbS (2), strongly indicating that this element of the crystal structure is preserved in the fibers. Therefore, a detailed description of the HbS fibers can now be attempted using the high-resolution information available for the crystal.

Several lines of evidence support the finding that elements of the crystal are present in the HbS fibers. X-ray diffraction (16, 17) and linear dichroism (18) studies of partially oriented specimens demonstrate features of the crystal paired strands in the fibers, and investigations using hybrid molecules having second amino acid substitutions show that regions involved in the axial and lateral contacts within the crystal pairs are important for fiber information (see refs. 3 and 4). In addition, crystal-like paired strands have recently been found in another, nonphysiological HbS polymer that can be formed by altering solution conditions (15). This observation further confirms the ability of the paired strand to assume a helical conformation.

The strong evidence for crystal and fiber similarities has led other investigators to propose 16- (6) or 14-strand (7) fiber models in which the pairing scheme has been altered to give a packing of double strands similar to that found in the crystals. A purportedly direct transition from fibers to the more stable crystal form (6, 17, 19) has been cited in support of these models. Additional models based on a comparison of calculated transforms with x-ray diffraction data also have been proposed (7). These various fiber models can be rejected for a number of reasons. The direct unwinding of fibers to form crystals has never been unambiguously established and thus should not be used as a criterion for evaluating fiber models. The 16-strand model is inconsistent with the results from embedded fibers presented here, which eliminates the possibility that additional strands are lost or disordered during the more severe adhesion preparation. Adding the extra two strands to the reconstructed fibers would also make their widths incompatible with x-ray diffraction results from packed gels (17). The data in this study clearly show the pairing schemes to be incorrect in the models based solely on the crystal structure and in some of the x-ray-based models. In addition, all of the alternate models deviate substantially from the fiber surface lattice that was established in early image-reconstruction studies (1, 5) and is confirmed, with minor modifications, in our current investigations (unpublished data). A much simplified comparison of model transforms with diffraction data from only moderately oriented fibers cannot justify large shifts of molecules from these positions. It should be noted, however, that the use of diffraction information may be helpful in extending models beyond the resolution of the EM data (20).

Although the packing of double strands in the fiber does not reproduce the crystal arrangement, the pairings and polarities now determined do suggest a relationship to a portion of the crystal. When viewed in cross section, the pairs 1–2, 3–4, and 10–11 have the same relative orientations and polarities as a three-pair section of the crystal (in the corresponding view along the *a* axis). This pattern is repeated for the pairs 6–7, 8–9, and 5–13 after a rotation of 180°. Thus, at least in the end-on view, the fiber appears to be composed of two crystal sections twisted into a helical conformation and linked by a seventh pair (12–14). Several pairs in the reconstructions also have relative axial positions that are equivalent to those of the corresponding crystal pairs (unpublished data). The crystals, then, may prove valuable for defining not only the interactions within pairs of strands but also many of the intermolecular contacts between pairs in the fiber. Success in modeling the molecular interactions in the HbS fibers should stimulate efforts to design antisickling agents and allow the relative merits of potential target sites to be evaluated (21).

We thank Margot Szalay for skillful preparation of the thin sections and assembling the figures, John Telford for the drawings, and Joyce Broadhead for typing the manuscript. This work was supported by grants from the National Institutes of Health and the American Heart Association. D.W.R. was a predoctoral fellow of the National Science Foundation.

1. Dykes, G., Crepeau, R. H. & Edelstein, S. J. (1978) *Nature (London)* **272,** 506–510.
2. Wishner, B. C., Ward, K. B., Lattman, E. E. & Love, W. E. (1975) *J. Mol. Biol.* **98,** 179–194.
3. Nagel, R. L., Johnson, J., Brookchin, R. M., Garel, M. C., Rosa, J., Schiliro, G., Wajcman, H., Labie, D., Moo-Penn, W. & Castro, O. (1980) *Nature (London)* **283,** 832–834.
4. Edelstein, S. J. (1981) *J. Mol. Biol.* **150,** 557–575.
5. Dykes, G. W., Crepeau, R. H. & Edelstein, S. J. (1979) *J. Mol. Biol.* **130,** 451–472.
6. Wellems, T. E. & Josephs, R. (1979) *J. Mol. Biol.* **135,** 651–674.
7. Rosen, L. S. & Magdoff-Fairchild, B. (1985) *J. Mol. Biol.* **183,** 565–574.
8. Crepeau, R. H. & Edelstein, S. J. (1984) *Ultramicroscopy* **13,** 11–18.
9. Pumphrey, J. G. & Steinhardt, J. (1976) *Biochem. Biophys. Res. Commun.* **69,** 99–105.
10. Mizuhira, V. & Futaesaku, Y. (1971) *Proc. Electron Microsc. Soc. Am.* **29,** 494–495.
11. Garrell, R. L., Crepeau, R. H. & Edelstein, S. J. (1979) *Proc. Natl. Acad. Sci. USA* **76,** 1140–1144.
12. Huisman, T. H. J. & Dozy, A. M. (1965) *J. Chromatogr.* **19,** 160–169.
13. Crepeau, R. H., Dykes, G., Garrell, R. L. & Edelstein, S. J. (1978) *Nature (London)* **274,** 616–617.
14. Crowther, R. A. & Klug, A. (1974) *Nature (London)* **251,** 490–492.
15. Potel, M. J., Wellems, T. E., Vassar, R. J., Deer, B. & Josephs, R. (1984) *J. Mol. Biol.* **177,** 819–839.
16. Magdoff-Fairchild, B., Swerdlow, P. H. & Bertles, J. F. (1972) *Nature (London)* **239,** 217–218.
17. Magdoff-Fairchild, B. & Chiu, C. C. (1979) *Proc. Natl. Acad. Sci. USA* **76,** 223–226.
18. Hofrichter, J., Hendricker, D. G. & Eaton, W. A. (1973) *Proc. Natl. Acad. Sci. USA* **70,** 3604–3608.
19. Makinen, M. W. & Sigountos, C. W. (1984) *J. Mol. Biol.* **178,** 439–476.
20. Rodgers, D. W., Crepeau, R. C. & Edelstein, S. J. (1986) in *Approaches to the Therapy of Sickle Cell Anemia,* eds. Beuzard, Y., Charache, S. & Galacteros, F. (Institut National de la Santé et de la Recherche Médicale, Paris), pp. 21–37.
21. Edelstein, S. J. (1985) *Annu. Rep. Med. Chem.* **20,** 247–255.